

2003

Kerr-resonance-condition-coupled enhancement in magneto-optic media

A. De
University of New Orleans

A. Puri
University of New Orleans

Follow this and additional works at: https://scholarworks.uno.edu/phys_facpubs



Part of the [Physics Commons](#)

Recommended Citation

J. Appl. Phys. 93, 1120 (2003)

This Article is brought to you for free and open access by the Department of Physics at ScholarWorks@UNO. It has been accepted for inclusion in Physics Faculty Publications by an authorized administrator of ScholarWorks@UNO. For more information, please contact scholarworks@uno.edu.

Kerr-resonance-condition-coupled enhancement in magneto-optic media

A. De and A. Puri^{a)}

Department of Physics, University of New Orleans, New Orleans, Louisiana 70148

(Received 8 August 2002; accepted 30 September 2002)

We derive an expression for cyclotron frequency ω_c , which sets $\text{Re}[\epsilon_+ \epsilon_-] = 1$ in a magneto-optic (MO) substrate, at any incident photon energy. Thereby, at any desired part of the optical spectrum, large Kerr effects can be obtained, which are generally known to occur either at the free-charge-carrier-plasma-resonance frequency ω_p , or at frequencies where active electronic transitions take place. Under these conditions, ω_p is seen to play a very different role; it is seen that for any ω , the magnitude of the Kerr resonance in a single MO (InSb here) substrate increases with decreasing ω_p . With the objective of achieving further Kerr enhancement, the effect of coating a thin film of this ω_c -coupled InSb layer on a Ag substrate is numerically studied. Further Kerr enhancement, at the plasma-resonance frequency of Ag, is seen, which is dependent on the thickness of the MO layer and its ω_p . In this configuration, giant resonances appear in the effective-dielectric-tensor spectra. The spectral locations of these resonances are dependent on the thickness of the MO layer. We interpret these resonance structures to be the effective cyclotron resonance. Our results suggest that there exists a strong correlation between the effective-cyclotron frequency and the plasma-resonance frequency of the noble. © 2003 American Institute of Physics. [DOI: 10.1063/1.1523141]

I. INTRODUCTION

Other than its use for the read out of magneto-optic (MO) digital storage systems, the magneto-optic Kerr effect (MOKE), particularly in the polar configuration, is one of the prime techniques to probe various magnetic properties, such as surface magnetism, multilayer-magnetic interlayer coupling and magnetic anisotropies.¹⁻³ Understanding the behavior of an optically active material begins with measurements that characterize material behavior. The resultant measurements can be explained, macroscopically, in terms of the dielectric tensor properties of the material, which are related to its band structure. This allows the Kerr effect to be used as a method to reveal details about electronic interband, as well as intraband, transitions,^{4,5} especially in transition-metal and rare-earth compounds. However, the origin of large MOKE still remains under dispute⁶ and has been attributed to numerous factors,^{5,7-9} mostly to active inter/intraband electronic transitions and to spin-orbit coupling. It has also been suggested that large resonance-shaped enhancements in the Kerr spectrum occur where $\text{Re}(\epsilon_{xx}) \approx 1$,¹⁰ which is mostly in the vicinity of the plasma-resonance frequency of free-charge carriers. In Ref. 11, we numerically studied the MOKE enhancement in a plasma resonance, $\text{Re}(\epsilon_{xx}) \approx 1$, coupled MO media in various thin-film configurations, where “ $\text{Re}(\epsilon_{xx}) = 1$ ” holds true at all incident photon energies. However, we have recently shown that in the event of a large reflection edge split, the resonance-shaped enhancements in the Kerr spectrum occur at $\text{Re}[\epsilon_+ \epsilon_-] \approx 1$ (Ref. 12) instead.

Therefore, in this article we derive an expression for the cyclotron frequency (which is dependent on the magnetic

field) in the framework of the Drude model, that satisfies the “ $\text{Re}[\epsilon_+ \epsilon_-] \approx 1$ ” resonance condition, and thus enables large Kerr rotations to be obtained at any given incident photon energy, which is not necessarily in the vicinity of either plasma-resonance-frequency or inter/intraband transitions.

In the case of MO layers embedded in metallic matrices, further enhancement of MOKE has been seen. This has been more widely attributed to the plasma resonance of free carriers in nonmagnetic noble metals,¹³⁻¹⁵ and to free electrons at the Fermi surface in quantum-well models.¹⁶⁻¹⁸ Hence, the cyclotron-frequency condition derived here is numerically coupled to a MO thin film, and its effects on the MOKE spectrum and the dielectric-tensor spectrum are studied by depositing it on a noble metal (NM) substrate.

The MO and NM selected here were InSb and Ag, respectively. Multiple reflection and interface effects within the medium were taken into account by using Fresnel's formulas. Some preliminary theoretical background for the free-charge-carrier Drude model and the derivations, are provided next, followed by discussion of the numerical results.

II. MACROSCOPIC THEORY OF POLAR MOKE

The dielectric response of a medium can be described by Maxwell's equations, whereby the propagation of an electromagnetic wave in a material can be described by the electric and magnetic permeability tensors ϵ and μ . Ignoring nonlinear effects and assuming that $\mu = 1$ at optical frequencies, the complex dielectric tensor can be simplified due to the symmetry in the configuration of the problem. In general, for most MO media, the dielectric tensor is symmetric in the absence of a magnetic field. This is particularly true for cubic crystals, where the dielectric tensor is symmetric about the optic axis and can be treated as a scalar. On the application

^{a)}Electronic mail: apuri@uno.edu

of a magnetic field in the z direction, the time reversal symmetry in the dielectric tensor is broken and can be expressed in terms of its dispersive and absorptive components as

$$\epsilon = \begin{pmatrix} \epsilon_{xx} & i\epsilon_{xy} & 0 \\ -i\epsilon_{xy} & \epsilon_{yy} & 0 \\ 0 & 0 & \epsilon_{zz} \end{pmatrix}. \quad (1)$$

The real component of the diagonal elements represent the ordinary optical absorption and the imaginary component of the off-diagonal elements represents the MO absorption, which is proportional to the difference in absorption between left and right circularly polarized light. Therefore, the eigenvalues of the dielectric function tensor can be expressed in terms of the complex index of refraction as

$$\tilde{n}_{\pm}^2 = \epsilon_{xx} \pm i\epsilon_{xy} = \epsilon_{\pm}. \quad (2)$$

Here, the “+” and “-” signs, respectively, represent right circularly polarized (RCP) and left circularly polarized (LCP) modes of wave propagation in a longitudinal magnetic field, \tilde{n}_{\pm} are the complex indices of refraction given by $\tilde{n}_{\pm} = n_{\pm} - ik_{\pm}$, and n_{\pm} and k_{\pm} are the refractive and absorptive parts, respectively. In the polar-Kerr configuration, the magnetization is perpendicular to the surface and parallel to the direction of light propagation. Since the eigenmodes are left and right circular polarizations, and therefore the Kerr resonance (KR), expressed as the phase different between the two circularly polarized modes,¹⁹ and the Kerr ellipticity (KE), expressed in terms of the complex reflection coefficients, are, respectively, given by

$$\theta_K = -\frac{1}{2}(\Delta_+ - \Delta_-), \quad \xi_K = -\frac{|r_+| - |r_-|}{|r_+| + |r_-|}. \quad (3)$$

Here,

$$r_{\pm} \text{ and } \Delta_{\pm} = \tan^{-1} \left(\frac{-2k_{\pm}}{n_{\pm}^2 + k_{\pm}^2 - 1} \right) = -j \log \frac{r_r^{\pm}}{|r_r^{\pm}|}$$

are the Fresnel’s reflection coefficients at normal incidence and the phase shifts, respectively, for LCP and RCP light.

Assuming that $(\Delta_+ - \Delta_-)$ is small and $(r_+ - r_-)^2 \ll 2r_+, r_-$, expressions for the complex polar MOKE given by Eqs. (3) and (4) can be approximated to²⁰

$$\Theta_k = \theta_k - i\xi_k = i \frac{\tilde{n}_+ - \tilde{n}_-}{\tilde{n}_+ \tilde{n}_- - 1}. \quad (4)$$

The Drude model is used here to describe the dielectric tensor components of a polar semiconductor. The independent particle model consists of free-charge carriers in the host lattice, which also contains an equal number of opposite charges to maintain charge neutrality. Random thermal motion of the free carriers is altered into cyclotron orbits in a plane perpendicular to the applied magnetic field. The application of a magnetic field also splits the plasma reflection edge into two. The spectral separation between the two reflectivity minima, increases linearly^{20,21} with increasing magnetic field, thus changing the complex index of refraction and inducing magnetic-circular birefringence, and magnetic-circular dichroism. In a polar semiconductor material such as InSb, the MO effects would be altered when lattice vibra-

tions are added. The changes are largest in the vicinity of the optical phonon frequencies. Hence, we can express the dielectric tensor in the polar-Kerr configuration, where Poynting vectors $\mathbf{S} \parallel \mathbf{B}_0$ and $\mathbf{E} \perp \mathbf{B}_0$ as¹

$$\epsilon_{\pm} = \epsilon_{\infty} \left(1 - \frac{\omega_p^2}{\omega(\omega \pm \omega_c - i\gamma)} + \frac{\omega_L^2 - \omega_T^2}{(\omega_T^2 - \omega^2 + i\Gamma\omega)} \right). \quad (5)$$

where, $\omega_p = (4\pi Ne^2/m^* \epsilon_c)^{1/2}$ is the plasma frequency, $\omega_c = He/m^*c$ is the cyclotron frequency; ϵ_{∞} is the background dielectric constant, ω_L is the longitudinal phonon frequency, ω_T is the transverse phonon frequency, Γ and γ are phonon damping constants, H is the magnetic field, c is the speed of light, e is the charge of an electron, m^* is the effective mass, N is the charge concentration, and ϵ_c is the dielectric constant of the medium.

The dielectric tensor for the two circular modes of propagation can be separated into its real and imaginary parts, respectively, as

$$\text{Re}(\epsilon_{\pm}) = \epsilon_{\infty} \left(1 - \frac{\omega_p^2(\omega \pm \omega_c)}{\omega[(\omega \pm \omega_c)^2 + \gamma^2]} + \frac{(\omega_L^2 - \omega_T^2)(\omega_T^2 - \omega^2)}{(\omega_T^2 - \omega^2)^2 + (\Gamma\omega)^2} \right), \quad (6a)$$

$$\text{Im}(\omega_{\pm}) = \omega_{\infty} \left(\frac{-\omega_p^2(\omega \pm \omega_c)}{\omega[(\omega \pm \omega_c)^2 + \gamma^2]} - \frac{\Gamma\omega(\omega_L^2 - \omega_T^2)}{(\omega_T^2 - \omega^2)^2 + (\Gamma\omega)^2} \right). \quad (6b)$$

In Ref. 12 we have shown that in the event of a large reflection edge split, a pronounced enhancement in the MOKE spectrum is expected in regions where $\text{Re}(\epsilon_+ \epsilon_-) \approx 1$, and not necessarily in the vicinity of the plasma resonance of the free-charge carriers. Hence, the first step in obtaining an expression for ω_c [where, $\text{Re}(\epsilon_+ \epsilon_-) \approx 1$ holds true for all ω and ω_p] would be to obtain an expression for $\text{Re}(\epsilon_+ \epsilon_-)$. By assuming that $\omega - \omega_c \gg \gamma$, we ignore γ^2 terms in Eqs. (6a) and (6b), and obtain

$$\text{Re}(\epsilon_+ \epsilon_-) = \epsilon_{\infty}^2 \left(1 + \frac{\omega_p^4}{\omega^2(\omega^2 - \omega_c^2)} - \frac{2(1+A)\omega_p^2}{\omega^2 - \omega_c^2} + A(2+A) \right), \quad (7)$$

where

$$A = \frac{(\omega_L^2 - \omega_T^2)(\omega_T^2 - \omega^2)}{(\omega_T^2 - \omega^2)^2 + \Gamma^2\omega^2}.$$

Thus, by substituting the $\text{Re}(\epsilon_+ \epsilon_-) \approx 1$ condition in Eq. (7) we obtain an expression for ω_c :

$$\omega_c = \left(\frac{\omega_p^4}{\omega^2(2A - X)} - \omega_p^2 \frac{1+A}{A - 0.5X} + \omega^2 \right)^{1/2}, \quad (8)$$

where

$$X = 1/\epsilon_{\infty}^2 - 1.$$

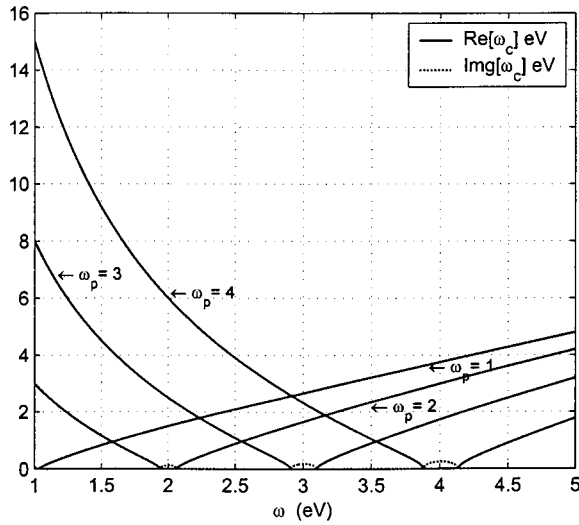


FIG. 1. Solution-curves showing real and imaginary parts of ω_c for various values of ω_p .

Therefore, if the cyclotron frequency (which is dependent on applied magnetic field, magnetization of the sample, and temperature) were made to vary as a function of incident photon energy according to Eq. (8), then a high KR could be obtained at any desired wavelength. Figure 1 shows the real and imaginary parts of ω_c for InSb as a function of ω_p and ω . The optical constants for InSb were obtained from Ref. 17. Upper- and lower-bound limits for ω_p can be calculated so as to keep ω_c real in the spectral window of interest. These constraining factors can be obtained by equating $\omega_c = 0$ in Eq. (8) and solving for ω :

$$\omega^2 = \frac{\omega_p^2}{A - X/2} \left(\frac{1+A}{2} \pm \sqrt{A^2 - 6A + 4X + 1} \right). \quad (9)$$

The solutions with the “-” sign gives the lower-bound limit and the solution with the “+” sign gives the upper-bound limit of the imaginary part of the curve in Fig. 1. The plasma frequency should be selected such that it is either greater than the highest incident photon energy or lesser than the lowest incident photon energy in the spectral window of interest. We select the lower-bound limit, as this is more physical. The maximum limit of plasma frequency for this material was set to be 0.9 eV so as to keep ω_c real.

III. NUMERICAL ANALYSIS

The numbers 0, 1, and 2 are assigned to air, MO semiconductor material (InSb), and noble metal (Ag), respectively. Dispersive effects are taken into account in the photon energy range of 1–5 eV for the refractive index of Ag,²² and the refractive indices of the InSb were calculated from Eq. (5), using the following optical constants: $\epsilon_\infty = 15.7$, $\omega_L = 19$ meV, $\omega_T = 17$ meV, $\Gamma = 1.2$ meV, and $\gamma = 0.6$ meV.²²

For any layered media, the polarized light beam experiences multiple reflections and interference effects in the thin-film layer. The resultant reflection coefficient conveys information about the overall amplitude and phase shifts and can be expressed as^{23,24}

$$r_r^\pm = \frac{r_{01}^\pm + r_{12}^\pm e^{-2j\beta_1^\pm}}{1 + r_{01}^\pm r_{12}^\pm e^{-2j\beta_1^\pm}}. \quad (10)$$

In the polar-Kerr configuration the magnetization is perpendicular to the surface and parallel to the direction of light propagation. The eigenmodes are left and right circular polarizations and thus the Fresnel's reflection coefficients at normal incidence of each interface are given by

$$r_{01}^\pm = \frac{1 - n_1^\pm}{1 + n_1^\pm} \quad \text{and} \quad r_{12}^\pm = \frac{n_1^\pm - n_2}{n_1^\pm + n_2}. \quad (11)$$

The phase factor is given by

$$\beta_i^\pm = \frac{2\pi}{\lambda} n_i^\pm d_i,$$

where d_i is the thickness of the i th layer, and the intensity reflectance of the layered system is $R_\pm = |r_r^\pm|^2$.

The KR and KE can, therefore, be obtained from the resultant reflection coefficients. A figure of merit (FOM) is commonly used to characterize the performance of a multilayer MO media. It is expressed as

$$\text{FOM} = \sqrt{\theta_k^2 R_a}, \quad (12)$$

where

$$R_a = \frac{|r_+^2| + |r_-^2|}{2}$$

is the average reflectivity.

In Fig. 2 various MOKE parameters, for the MO substrate, 01 configuration, were plotted as a function of wavelength and for various ω_p (0.2 eV, 0.8 eV). The KR as seen in Fig. 2(a) is significantly higher for $\omega_p = 0.2$ eV. At $\omega_p = 0.8$ eV, the KR is nearly flat and is around $\sim 1.6^\circ$ and also has very small KE throughout the optical spectrum. For $\omega_p = 0.2$ eV, the KE curve is much higher and also the difference in the reflectivity for LCP and RCP is much larger than at $\omega_p = 0.8$. In general, for the 01 configuration, the FOM for $\omega_p = 0.2$ eV is relatively higher as compared to the $\omega_p = 0.2$ eV case.

The effect of depositing a thin film of MO on a noble substrate (012 configuration) is studied next. The KR is expected to increase in this configuration, as the plasma resonance of free-charge carriers in the nonmagnetic metal (i.e., where optical constants n_{Ag} and k_{Ag} are the lowest) would alter the effective dielectric constant, which would aid in the KR enhancement, accompanied by an enhancement in KE.

First we plot a three-dimensional graph for the KR and average reflectivity, as shown in Fig. 3. This is done at $\omega_p = 0.8$ eV to show the simultaneous effect of varying ω and d_1 on the KR and average reflectivity. It is seen that higher KR are seen only at certain incident photon energies. The KR is $\sim 0^\circ$ at 1 eV for all d_1 , however, it experiences a sharp rise as the incident photon energy is increased. The spectral occurrence of this rise is dependent on d_1 . At the same time notice that the average reflectivity experiences minima in the vicinity of the rise in the KR.

The thickness-dependent behavior of the MO layer on the Ag substrate is examined in greater detail in the next set

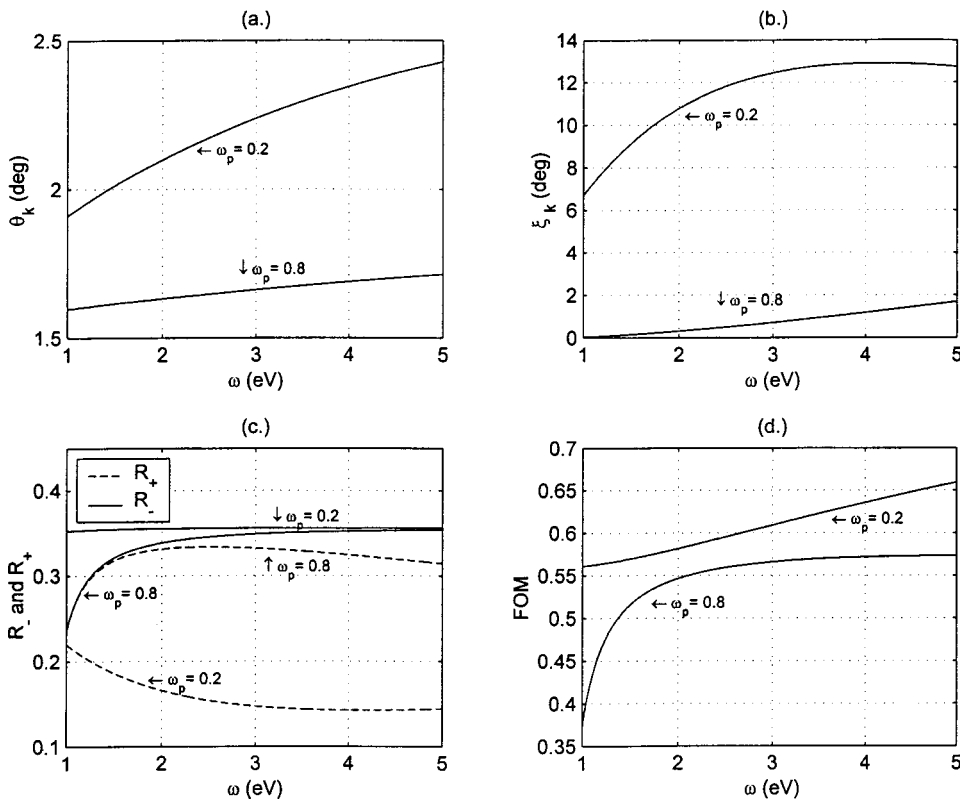


FIG. 2. (a) Kerr rotation, (b) Kerr ellipticity, (c) reflectivity, and (d) FOM for the 01 configuration.

of graphs. In Fig. 4, we shown various MOKE parameters at $d_1 = 15$ nm. Several interesting features are observed, most notably the KE. Notice that in Fig. 4(b) a very sharp resonance-like structure in the KE spectrum is observed at

the plasma resonance of Ag (~ 3.8 eV). Similarly, in Fig. 4(a) the KR experiences a rise around the plasma resonance of Ag. However, unlike in the case of the KE spectrum this enhanced KR value remains locally invariant 3.8 eV onwards. In Fig. 4(c), notice that the reflection spectra for RCP light closely resembles that of Ag near its plasma edge. The LCP reflectivity for the different ω_p values is nearly indistinguishable. Overall, lower ω_p resulted in higher MOKE.

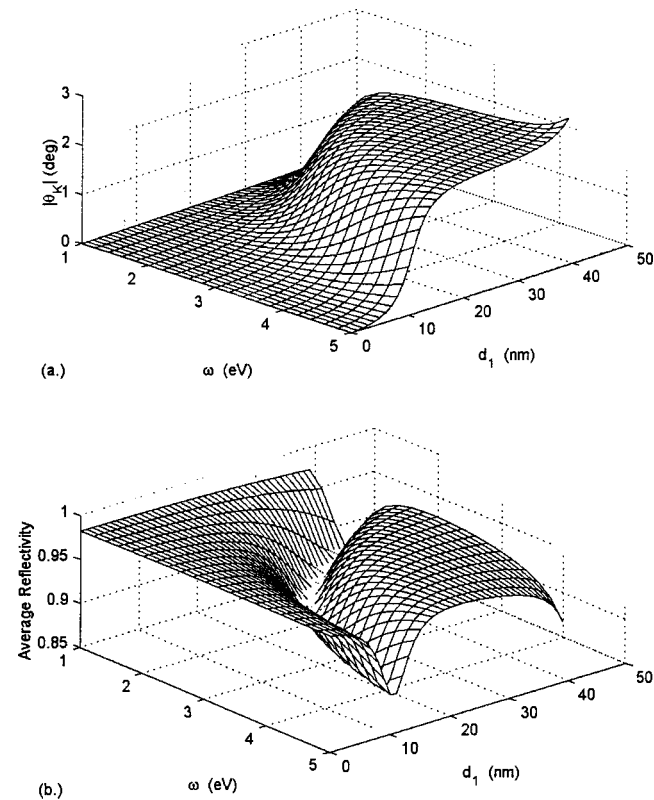


FIG. 3. (a) Kerr rotation and (b) average reflectivity as a function of ω and d_1 , for the 012 configuration at $\omega_p = 0.8$ eV.

A further analysis of the 012 configuration is carried out at $d_1 = 40$ nm in Fig. 5. In Fig. 5(a), it is shown that a further enhancement of KR is observed at ~ 3.8 eV. The KR for $\omega_p = 0.2$ is greater than 3° . The local invariance seen in the earlier KR figure is not seen any more around 3.8 eV, instead a sharply rising peak is observed. In Fig. 5(b) it is seen that the KE experiences a sharp resonance and rapidly changes sign around 3.8 eV. The reflectivity for LCP is nearly invariant with respect to ω_p and bears very close resemblance to that of a Ag substrate. The RCP shows a significantly different response to different ω_p , and it, too, experiences a minimum at the plasma resonance of Ag. It is important to point out that under the present ω_c -coupled MO layer conditions, the magnitude of the Kerr enhancement is dependent on the plasma resonance of the MO layer, and that lower ω_p results in higher MOKE, especially at the plasma resonance of Ag. Overall, it is seen that when $d_1 = 40$ nm, the FOM increases sharply at lower ω . However, it also experiences a sharper decline at the plasma-resonance frequency of Ag as compared to $d_1 = 15$ nm.

An interesting phenomenon is seen in the spectra of the effective ϵ_{xx} and ϵ_{xy} in Fig. 6, which were calculated from resultant reflectivity R_r . Giant resonance are seen in the

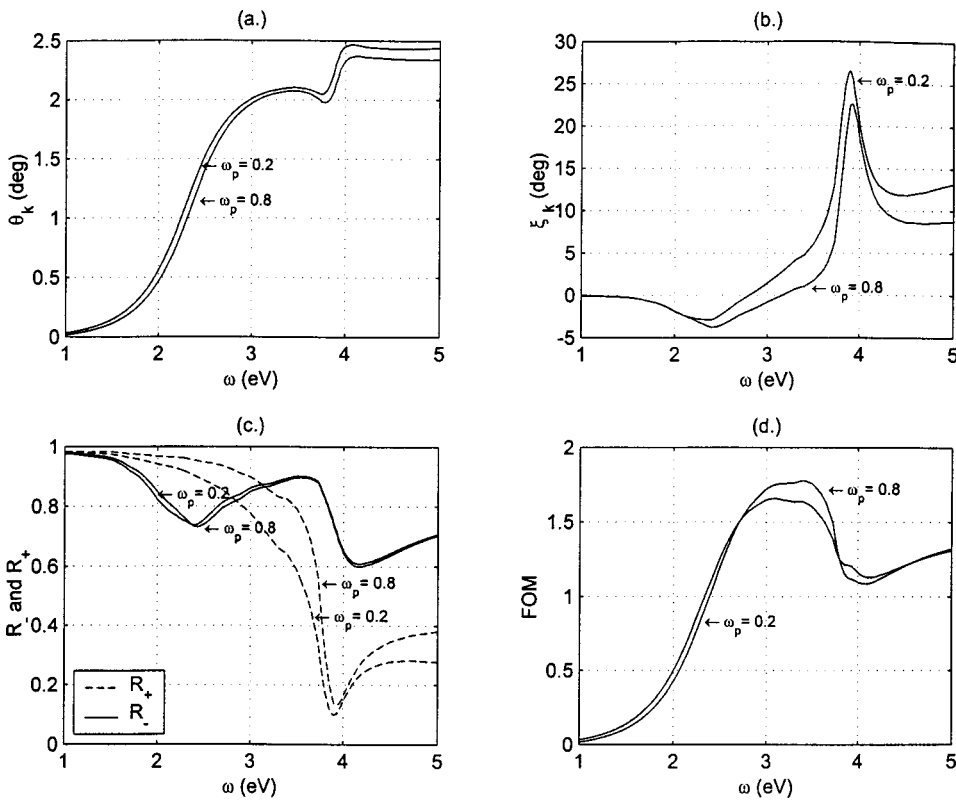


FIG. 4. (a) Kerr rotation, (b) Kerr ellipticity, (c) reflectivity, and (d) FOM for the 012 configuration at $d_1=15$ nm, $\omega_p=0.8$ eV.

effective-dielectric-tensor spectrum for $\omega_p=0.8$ eV. The spectral locations of these resonance vary with thickness d_1 and occur at longer wavelengths and become sharper with increasing d_1 . In Fig. 7, the spectral locations of these resonances are plotted as a function of thickness d_1 ; subtle varia-

tions are also noted with respect to ω_p . We interpret these resonances as the effective-cyclotron resonance, since the cyclotron-resonance effect is generally seen only in the dielectric tensor spectra because of the functional form of ϵ_{xx} and ϵ_{xy} , in the free-carrier Drude model.²⁵ Hence, under the

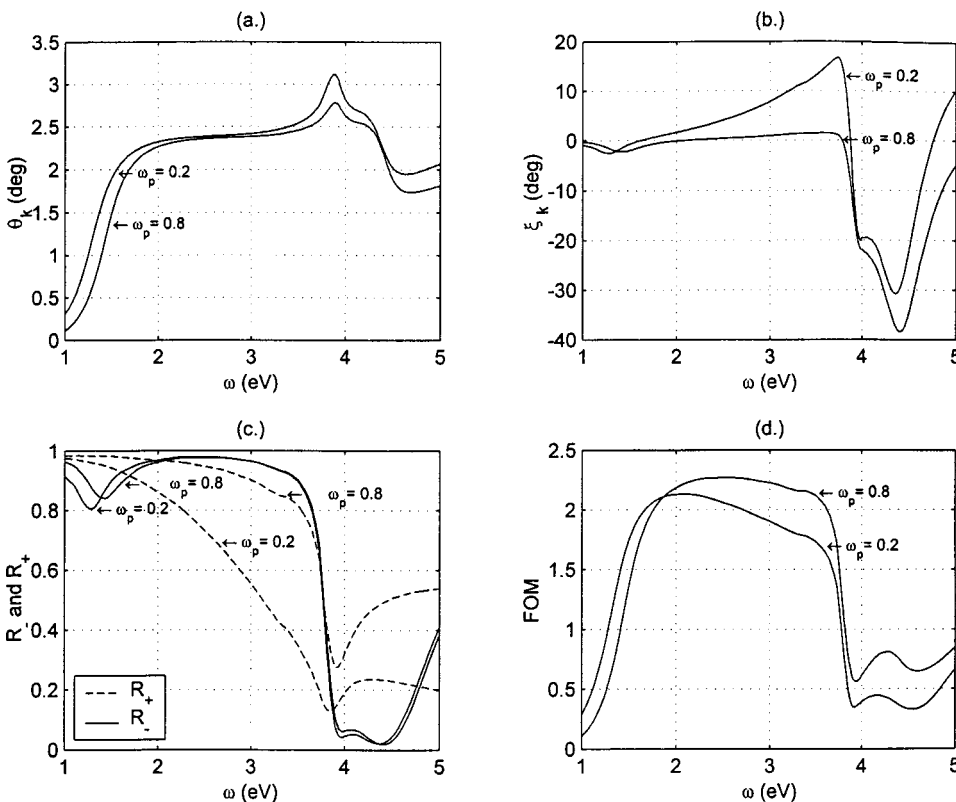


FIG. 5. (a) Kerr rotation, (b) Kerr ellipticity, (c) reflectivity, and (d) FOM for the 012 configuration at $d_1=15$ nm, $\omega_p=0.8$ eV.

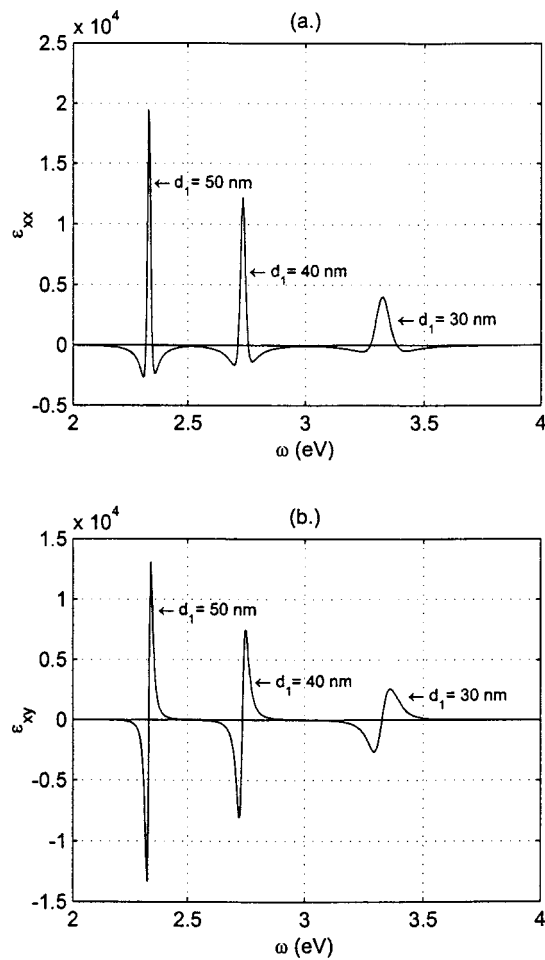


FIG. 6. Effective-dielectric-tensor spectra for the 012 configuration at $\omega_p = 0.8$ eV.

present conditions for the 012 configuration an effective-cyclotron frequency can be generated simply by varying the thickness of the MO layer. Our results suggest that as the thickness of the MO layer decreases, the spectral limit of the effective-cyclotron frequency is shifted towards the plasma-resonance frequency of the noble metal as its maximum

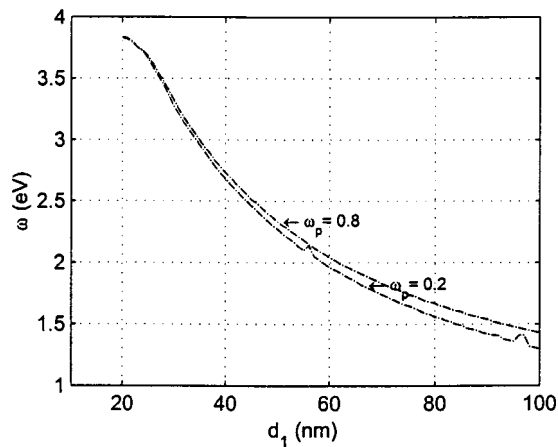


FIG. 7. Spectral location of effective-cyclotron resonance as a function of MO-layer thickness d_1 for the 012 configuration.

upper-bound value, beyond which no such resonances are observed.

IV. SUMMARY

In this article, we derived an expression for cyclotron frequency ω_c , which sets $\text{Re}[\epsilon_+ \epsilon_-] = 1$ in the MO medium at any incident photon energy, and thus high KR can be obtained at any desired wavelength. Therefore, even though high KR are known to occur at either free-charge-carrier-plasma resonance frequency ω_p , or at frequencies where active electronic transitions take place, we have shown that under framework of the Drude model (by appropriate coupling of ω and ω_c) enhanced MOKE can be achieved at any desired part of the optical spectrum, as seen in Fig. 2. Under these conditions, it is seen that the magnitude of the KR in a single MO (InSb here) substrate has a sensitive dependence on the choice of ω_p , the lower numerical value of which results in higher KR.

The MOKE study was extended to the MO-layer/noble-metal configuration, where the surface plasmon of the noble metal (Ag here) is known to enhance the KR at its plasma resonance frequency. This is seen to be true for this configuration, even under the present ω_c -coupling conditions. The magnitude of the KR enhancement at the noble-metal-plasma-resonance frequency was, however, seen to be dependent on the thickness of the MO layer and its ω_p . In the effective ϵ_{xx} and ϵ_{xy} spectra, giant resonances are seen, which are MO-layer-thickness dependent. We interpret these resonance-like structures to be the effective-cyclotron resonance. This conclusion is deduced from the functional form of dielectric tensor elements, in the free-carrier-Drude model. Hence, under the present conditions and in the present configuration, an effective-cyclotron frequency can be generated, simply by varying the thickness of the MO layer. Our results suggest that in the limit of minimum MO-film thickness, the spectral location of the effective-cyclotron resonance approaches the plasma-resonance frequency of Ag. This conclusion was also verified by considering a generic model for noble metals.

¹C. Liu, E. R. Moog, and S. D. Bader, Phys. Rev. Lett. **60**, 2422 (1988).
²W. R. Bennet, W. Schwarzacher, and W. F. Egelhoff, Phys. Rev. Lett. **65**, 4971 (1989).
³W. B. Zeper, F. J. A. M. Greidanus, P. F. Garcia, and C. R. Fincher, J. Appl. Phys. **65**, 4971 (1989).
⁴H. S. Bennet and E. A. Stern, Phys. Rev. **137**, A448 (1965).
⁵J. L. Erskine and B. R. Cooper, Phys. Rev. B **8**, 1239 (1973).
⁶P. M. Oppeneer, T. Maurer, J. Sticht, and J. Kubler, Phys. Rev. B **45**, 10924 (1994).
⁷R. A. de Groot, F. M. Muller, P. G. van Engen, and K. H. J. Bushow, Phys. Rev. Lett. **50**, 2024 (1983).
⁸J. H. Wijnngaard, C. Hass, and R. A. de Groot, Phys. Rev. B **40**, 9318 (1989).
⁹H. S. Bennet and E. A. Stern, Phys. Rev. **137**, A448 (1965).
¹⁰H. Fiel and C. Haas, Phys. Rev. Lett. **58**, 65 (1988).
¹¹A. De and A. Puri, J. Appl. Phys. **91**, 9777 (2002).
¹²A. De and A. Puri, J. Appl. Phys. **92**, 5401 (2002).
¹³P. M. Oppeneer, T. Maurer, J. Sticht, and J. Kubler, J. Phys.: Condens. Matter **6**, 285 (1994).
¹⁴T. Katayama, Y. Suzuki, H. Awano, Y. Nishihara, and N. Koshizuka, Phys. Rev. Lett. **60**, 1426 (1988).
¹⁵W. Reim and D. Weller, Appl. Phys. Lett. **53**, 2453 (1988).
¹⁶M. D. Stiles, Phys. Rev. B **48**, 7238 (1993); P. Bruno, *ibid.* **46**, 261 (1992).

- ¹⁷B. A. Jones and C. B. Hanna, Phys. Rev. Lett. **71**, 4253 (1993).
- ¹⁸A. Carl and D. Weller, Phys. Rev. Lett. **74**, 190 (1995).
- ¹⁹K. Egashira and T. Yamada, J. Appl. Phys. **45**, 3643 (1974).
- ²⁰W. Reim and J. Schones, *Magneto-Optical Spectroscopy, Ferromagnetic Materials* (Elsevier Science, New York, 1990), Vol. 5.
- ²¹S. J. Buchsbaum, in Proceedings of the International Conference on the Physics of Semiconductors Symposium on the Plasma Effect in Solids, Dunod, Paris (1964).
- ²²*Handbook of Optical Constants of Solids*, edited by E. D. Palik (Academic, New York, 1996).
- ²³R. Fang, C. Peng, T. Ma, P. Long, J. Liu, Y. Nin, and D. Dai, J. Appl. Phys. **74**, 6830 (1993).
- ²⁴R. M. A. Azzam and N. M. Bashara, *Ellipsometry and Polarized Light* (Elsevier Science, Amsterdam, 1987).
- ²⁵J. G. Mavroides, *Optical Properties of Solids*, edited by F. Abeles (North-Holland, Amsterdam, 1972), Chap. 7.